The Importance of Cantilever Dynamics in the Interpretation of Kelvin Probe Force Microscopy

The importance of cantilever dynamics in the interpretation of Kelvin probe force microscopy

Kevin J. Satzinger,[1] Keith A. Brown,[2,b] and Robert M. Westervelt[2,3,a]

[1]Truman State University, Department of Physics, Kirksville, MO 63501

[2]Harvard University School of Engineering and Applied Sciences, Cambridge, MA 02138

[3]Department of Physics, Harvard University, Cambridge, MA 02138

[a]Electronic mail: westervelt@seas.harvard.edu

[b]Current Address: International Institute for Nanotechnology, Northwestern University, Evanston, IL 60208

A realistic interpretation of the measured contact potential difference (CPD) in Kelvin probe force microscopy (KPFM) is crucial in order to extract meaningful information about the sample. Central to this interpretation is a method to include contributions from the macroscopic cantilever arm, as well as the cone and sharp tip of a KPFM probe. Here, three models of the electrostatic interaction between a KPFM probe and a sample are tested through an electrostatic simulation and compared with experiment. In contrast with previous studies that treat the KPFM cantilever as a rigid object, we allow the cantilever to bend and rotate; accounting for cantilever bending provides the closest agreement between theory and experiment. We demonstrate that cantilever dynamics play a major role in CPD measurements and provide a simulation technique to explore this phenomenon.

I. Introduction

Electrostatic force microscopy (EFM) is a widely used technique for nanoscale electrical characterization.[1-3] Among the many EFM techniques, Kelvin probe force microscopy (KPFM) has proven to be a powerful technique to measure the local work function.[4-7] A central challenge in KPFM is to achieve nanoscale spatial resolution, despite the large size of the probe and the long range of the electrostatic interaction.[8-10] While modifications to the basic KPFM experimental technique exist to improve spatial resolution,[8,11-13] in many circumstances the measurement is complicated through the electrostatic contributions from the macroscopic cantilever of the probe. Theoretical studies have been used extensively to analyze the resolution of EFM techniques such as KPFM. The electrostatics of the tip of a probe has been studied independently,[14-16] and the cantilever has been included as a cylindrical plate,[17] a square box,[18] and as a full three-dimensional cantilever.[8,19-21] Recently, it has become apparent that the dynamics of the cantilever are important when considering electrostatic forces.[22]

In this work, we demonstrate a novel method to simulate KPFM that includes the dynamics of the cantilever arm. We first overview the operating principles of KPFM and describe the fabrication of an experimental step sample. We then simulate the ideal KPFM step function at the boundary between two different materials using a finite-element electrostatic method that takes into account three models of cantilever dynamics: translation, rotation, and bending. The dynamics of the cantilever arm is found to be important, and increasing the realism of the model of cantilever dynamics greatly improves the agreement with experiment.

II. Kelvin Probe Force Microscopy

In KPFM, we seek to map the tip-sample contact potential difference (CPD) V_C.[4] A conducting probe is brought within a few 10's of nm of a sample surface, and the probe-sample system is treated as a capacitor with capacitance C. The vertical component of the electrostatic force F on the probe is given by,

$$F = \frac{1}{2}\frac{\partial C}{\partial z}\left(V - V_C\right)^2, \tag{1}$$

where z is the vertical tip-sample distance, and V is the applied voltage between the probe and sample. By setting $V = V_{DC} + V_{AC}\sin(\omega t)$, the force will have a DC term, a term that oscillates at ω (with amplitude F_ω), and a term that oscillates at 2ω. The cantilever mechanical resonance angular frequency ω_0 is utilized to amplify F_ω by setting $\omega = \omega_0$. We adjust V_{DC} in a feedback loop to null F_ω. We define the value of V_{DC} for which $F_\omega = 0$ as the Kelvin voltage V_K. In the case of a uniform sample, $V_K = V_C$.

In a real KPFM experiment, the probe may interact with multiple regions i of the sample with different CPDs V_{Ci}. In this case, we treat the probe-sample interaction as a set of parallel capacitances,[17] each with capacitance C_i. The total vertical component of the electrostatic force F on the probe is given by,

$$F = \sum_i \frac{1}{2}\frac{\partial C_i}{\partial z}\left(V - V_{Ci}\right)^2, \tag{2}$$

Applying the KPFM technique by adjusting V_{DC} to null F_ω gives,

$$V_K = \frac{\sum_i V_{Ci}\left(\partial C_i/\partial z\right)}{\sum_i \left(\partial C_i/\partial z\right)}, \tag{3}$$

In which V_K is a weighted average of the local CPDs. The probe is scanned across the sample surface to obtain a map of V_K representing the local CPD.

III. Experimental Procedure

Metallic KPFM calibration samples were fabricated with photolithography, as shown in Fig. 1(a), with a schematic side view in Fig. 1(b). First, a heavily n-doped Si wafer (Silicon Quest International, Inc.) is coated with an insulating layer consisting of ~ 400 nm of SiO_2 and ~ 100 nm of Si_3N_4 by low-pressure chemical vapor deposition to form an insulating substrate. Wafer chips are then chemically cleaned, a photoresist is spun on, and a 100 μm wide strip is patterned with photolithography. Electron beam evaporation is used to deposit 10 nm of Ti followed by 50 nm of Au to form a long strip electrode. A focused ion beam (NVision 40 - Carl Zeiss Inc.) is used to mill a ~ 500 nm wide trench across the electrode to make two electrically insulated electrodes. In this configuration, we have two electrodes to which we can apply independent potentials -1 V to the first and 1 V to the second, as indicated in Fig. 1(b). The choice of Au is ideal as it does not oxidize readily. The electrode configuration and large potential difference minimize the effects of surface charging on the KPFM measurement. Additionally, comparing the same material held at two different potentials is found to be more reproducible than comparing two materials with different work functions.

KFPM measurements are performed as two-pass measurements using a commercial AFM system (MFP-3D - Asylum Research) and commercial EFM probes (Arrow-NCPt - NanoWorld AG). KPFM scans are taken over the maximum lateral range 90 μm with the tip held 50 nm above the sample, with the result indicated in Fig. 1(c). An average line scan is found by centering lines of V_K together about the topographic feature at the step and averaging.

IV. Electrostatic Simulation

We performed finite-element electrostatic simulations of KPFM measurements of V_K, by calculating the capacitance C_i between a realistic EFM probe model and each region i of the sample. By calculating C_i for many values of tip-sample separation z, we estimate $\partial C_i/\partial z$ using a finite-difference method. These derivatives are used with Eq. (3) to calculate V_K. To simulate a KPFM scan, we repeat the same procedure at different lateral positions x along the sample. Cantilever dynamics are incorporated by controlling the displacement profile of the cantilever at a given z, including cantilevers that translate, rotate, or bend.

Three-dimensional (3D) finite-element electrostatic simulations (Maxwell 11 - Ansys Inc.) of the capacitances C_i between a probe and the two half-planes, are shown in Fig. 2(a). Finite-element simulation is necessary to determine the capacitances due to the complicated geometry in the simulation.[23] The 3D probe model is constructed from manufacturer specified parameters of the probe used in the experiment; an image of the actual probe and the probe model are compared in Fig. 2(b). The tip of the probe is truncated in the model, terminating in a triangular surface with sides of length 10 nm parallel to the sample surface, as shown in Fig. 2(c). This tip size is commensurate with the specified tip radius. The probe is positioned with its tip 50 nm from the surface and with the cantilever tilted 11º with respect to the sample, as in our experimental setup. During simulations, the probe is held at 1 V while the substrate and boundaries are grounded.

To overcome the difficulty imposed the large discrepancy of length scales in the simulation[10] (cantilever length 160 μm *vs*. tip-sample separation 50 nm), we separate the cantilever and cone, as indicated in Fig. 2(b). As depicted in Fig. 2(a), the cantilever simulation consists of two adjacent 1 × 1 mm^2 squares forming the substrate with the simulation volume extending 1 mm above the substrate, while the cone simulation consists of two 400 × 400 μm^2 squares with the simulation volume extending 100 μm upward. The total capacitance between the probe and each sample region is given by $C_i = C_i^{cone} + C_i^{cant}$, where C_i^{cone} is the cone- substrate capacitance with the cantilever removed, while C_i^{cant} is the cantilever-substrate capacitance with the cone removed. We analyze the effect of treating the cone and cantilever separately by considering the capacitance between the probe and the entire sample region. In this simplified simulation, where only one probe-sample capacitance is present, we are able to simulate the entire probe (cone and cantilever) at once. We consider the change in probe-sample capacitance

ΔC with the change in probe-sample displacement Δz, comparing the result from the simulation of the whole probe to the result from simulating the cone and cantilever separately and adding their capacitances together. Determining $\partial C_i/\partial z$ for each case, we observe only small discrepancies between the whole-probe simulation and the split-probe simulations of 0.1% for translation, 5% for rotation, and 2% for bending.

We calculate V_K by approximating $\partial C_i/\partial z$ between the probe and each region of the substrate. Capacitances C_1 and C_2 are calculated over a range of tip-sample separations z and fit the resultant function to a power law, as shown in Fig. 3(a) for the cone and Fig. 4(b) for the cantilever. The power law fit allows us to extract $\partial C_i/\partial z$ at a particular x value. By assigning values to V_1 and V_2, we may use Eq. (3) to find the predicted Kelvin voltage V_K. We repeat these steps for x from -100 μm to 250 μm to simulate a KPFM line scan. We also employ phenomenological fitting of $\partial C_i/\partial z$ *vs*. x to analytic functions for further analysis. The curve $\partial C_i^{cone}/\partial z$ *vs*. x is found to fit well to a sum of two Gompertz functions,[24] shown in Fig. 3(b).

We incorporate cantilever dynamics by modifying the cantilever deflection profile and observe a strong change in $\partial C/\partial z$. The deflection of the cantilever can be parameterized as the deviation $\delta(y)$ from rest at a position y along the axis of the cantilever, where $y = 0$ corresponds to the fixed end of the cantilever and $y = L$ corresponds to the free end. We consider three cantilever deflection profiles $\delta(y)$ that determine the physical interaction we are considering, which are illustrated in Fig. 4(a). (1) The translation method is what has been used previously - here the cantilever moves uniformly ($\delta(y) = z$). (2) The rotation method takes into account that the fixed end is immobile and allows the cantilever to rotate about it ($\delta(y) = z\ (y/L)$). (3) The bending method has the cantilever obey the Euler-Bernoulli beam equations;[25] $\delta(y) = z\, f(y)$ where $f(y)$ is the first normal mode given as Eq. (8) in Ref. 25. The deflection profiles are enforced by defining the cantilever deflection parametrically. The curve $\partial C/\partial z$ *vs*. x for each of these methods is plotted in Fig. 4(c-e) and fit to a linear function times a logistic function added to a Gompertz function times a logistic function.[26]

V. Results and Discussion

The cantilever plays a large role in KPFM experiments, as demonstrated by the similarity of the simulated magnitudes of $\partial C/\partial z$ for the cone and cantilever. The maximum absolute value of $\partial C^{cone}/\partial z$ estimated from fitting Fig. 3(b) is $\partial C^{cone}/\partial z = 0.118$ fF μm^{-1}. In contrast, $\partial C/\partial z$ for the cantilever undergoing translation, rotation, and bending, found from Fig. 4(c), Fig. 4(d), and Fig. 4(e) respectively, gives $\partial C^{trans}/\partial z = 0.139$ fF μm^{-1}, $\partial C^{rot}/\partial z = 0.080$ fF μm^{-1}, and $\partial C^{bend}/\partial z = 0.066$ fF μm^{-1}. Because these values are of similar size, no matter the model of cantilever dynamics used, cantilever and the cone will play similar roles in determining the measured value of the CPD.

Increasing the realism of the modeled cantilever dynamics (from translation to rotation and finally to bending) improves the agreement with experimental data, as shown in Fig. 5. The cantilever is oriented with the base toward the left and the tip on the right. The experimental step in V_K between the two electrodes is shown in Fig. 5 along with the simulated steps for translating, rotating, and bending cantilevers calculated using Eq. (3). While the simulated traces show good agreement for $x < 0$ while the entire probe is held above one electrode, they show significant disarrangement with the experimental data for $x > 0$ while the cantilever arm is gradually crossing the step between the two electrodes. All simulated traces fall below the experimental data, indicating that the contribution for the cantilever is overestimated. The large variation in the simulated traces for $x > 0$ demonstrates that picking the correct mode of cantilever dynamics is of high importance. Increasing the realism of the model greatly helps agreement with experiment.

The discrepancy between the most realistic model of cantilever dynamics and the experimental data likely comes from differences in the simulated and experimental systems. Experimental traces of V_K were consistently seen to reach higher voltages than theoretically predicted at a given distance from the step, indicating that the theoretical treatment over-emphasized the contribution of the cantilever. The equation of bending used here is precise for a beam with a uniform rectangular cross section. Modifying the bending profile to be accurate for the arrow-style probe shown in Fig. 1(b) would improve agreement. Further, while breaking up the probe into cantilever and cone sections is necessary due to computational restrictions, it introduces x-dependent error. Noncontact friction interactions have been observed between metal-coated cantilevers and metal surfaces; the effect is especially pronounced for $z < 10$ nm.[27]

Cantilever vibration itself displaces charge, damping the vibration, and changing electromagnetic fields induce Casimir forces that are significant for small z.[28] These effects are not taken into account in our electrostatic simulations, and CPD measurements taken with small probe-sample separations and inhomogeneous samples would display these effects.

Our simulation methodology can also be used to provide insight into frequency modulated KPFM[5] (FM-KPFM) and explain the improvement in spatial resolution that is achieved. FM-KPFM, in which V_K depends on $\partial^2 C/\partial z^2$, has superior spatial resolution to standard amplitude-modulated KPFM (AM-KPFM), which can be explained by the near linear relationship between C^{cant} and z. Although this dependence of C^{cant} on z introduces a significant contribution of the cantilever to AM-KPFM measurements, where $\partial C/\partial z$ is important, the second derivative $\partial^2 C/\partial z^2$ for the cantilever is quite small. Hence the contribution of the cantilever in this alternative technique will not be as significant. Although the cantilever interacts with the sample *via* long-range interactions, the extent to which long range interactions affect the measurement depends greatly on the technique in use.

In summary, we have developed a method to simulate KPFM measurements that includes three models of cantilever dynamics, and we have used this method to demonstrate the importance of cantilever dynamics. Through comparison of finite-element simulations with experiment, we find that improving the realism of the model of cantilever dynamics significantly increased agreement with experimental results. Our analysis here has centered around amplitude modulated KPFM, but these findings and methods are relevant to any AFM technique that uses a long-range interaction, including other types of EFM and Magnetic Force Microscopy.[29]

Acknowledgements

The authors thank Michael Goggin and Eduardo Velasco for their assistance with computing resources, Rafael Jaramillo for helpful discussions, and Kathryn Hollar for logistical support. We acknowledge support by the National Nanotechnology Infrastructure Network through the Research Experience for Undergraduates Program through National Science Foundation grant number ECCS-0821565 and the Department of Energy through grant number DE-FG02-07ER46422.

References

[1]P. Girard, "Electrostatic force microscopy: principles and some applications to semiconductors," *Nanotech.*, **12**, 485-490 (2001).

[2]S. V. Kalinin, R. Shao, and D. A. Bonnell, "Local pheonomena in oxides by advanced scanning probe microscopy," *J. Am. Ceram. Soc.*, **88**, 1077-1098 (2005).

[3]R. A. Oliver, "Advances in AFM for the electrical characterization of semiconductors," *Rep. Prog. Phys.*, **71**, 076501 (2008).

[4]M. Nonnenmacher, M. P. O'Boyle, and H. K. Wickramasinghe, "Kelvin probe force microscopy," *Appl. Phys. Lett.*, **58**, 2921-2923 (1991).

[5]J. L. Luria, K. A. Schwarz, M. J. Jaquith, R. G. Hennig, and J. A. Marohn, "Spectroscopic characterization of charged defects in polychristalline pentacene by time- and wavelength-resolved electric force microscopy," *Adv. Mater.*, **20**, 1-5 (2010).

[6]H. R. Moutinho, R. G. Dhere, C.-S. Jian, Y. Yan, D. S. Albin, and M. M. Al-Jassim, "Investigation of potential and electric field profiles in cross sections of CdTe/CdS solar cells using scanning Kelvin probe microscopy," *J. Appl. Phys.*, **108**, 074503 (2010).

[7]R. Jaramillo and S. Ramanathan, "Kelvin force microscopy studies of work function of transparent conducting ZnO:Al electrodes synthesized under varying oxygen pressures," *Sol. Energy Mater. Sol. Cells*, **95**, 602-605 (2011).

[8]J. Colchero, A. Gil, and A. M. Baro, "Resolution enhancement and improved data interpretation in electrostatic force microscopy," *Phys. Rev. B*, **64**, 245403 (2001).

[9]T. Glatzel, S. Sadewasser, R. Shikler, Y. Rosenwaks, and M. C. Lux-Steiner, "Kelvin probe force microscopy on iii-v semiconductors: the effect of surface defects on the local work function," *Mat. Sci. Eng. B*, **102**, 138-142 (2003).

[10]G. M. Sacha, E. Sahagun, and J. J. Saenz, "A method for calculating capacitances and electrostatic forces in atomic force microscopy," *J. Appl. Phys.*, **101**, 024310 (2007).

[11]C. Sommerhalter, T. W. Matthew, T. Glatzel, A. Jager-Waldau, and M. C. Lux-Steiner, "High-sensitivity quantitative Kelvin probe microscopy by noncontact ultra-high-vacuum atomic force microscopy," *Appl. Phys. Lett.*, **75**, 286-288 (1999).

[12]F. Kork, K. Sajewicz, J. Konior, M. Goryl, P. Piatkowski, and M. Szymonski, "Lateral resolution and potential sensitivity in Kelvin probe force microscopy: Towards understanding of the sub-nanometer resolution," *Phys. Rev. B*, **77**, 235427 (2008).

[13]K. A. Brown, K. J. Satzinger, and R.M. Westervelt, "High spatial resolution Kelvin probe force

microscopy with coaxial probes" *Nanotechnology* **23**, 115703 (2012).

[14]S. Hudlet, M. S. Jean, C. Guthmann, and J. Berger, "Evaluation of the capacitive force between at atomic force microscope tip and a metallic surface," *Eur. Phys. J. B*, **2**, 5-10 (1998).

[15]S. Gomez-Monivas, L. S. Froufe, R. Carminati, J. J. Greffet, and J. J. Saenz, "Tip-shape effects on electrostatic force microscopy resolution," *Nanotech.*, **12**, 496-499 (2001).

[16]T. Machleidt, E. Sparrer, D. Kapusi, and K.-H. Franke, "Deconvolution of Kelvin probe force microscopy measurements - methodology and application," *Meas. Sci. Technol.*, **20**, 084017 (2009).

[17]H. O. Jacobs, P. Leuchtmann, O. J. Homan, and A. Stemmer, "Resolution and contrast in Kelvin probe force microscopy," *J. Appl. Phys.*, **84**, 1168-1173 (1998).

[18]S. Sadewasser, T. Glatzel, R. Shikler, Y. Rosenwaks, and M. C. Lux-Steiner, "Resolution of Kelvin probe force microscopy in ultrahigh vacuum: comparison of experiment and simulation," *Appl. Surf. Sci.*, **210**, 32-36 (2003).

[19]S. Belaidi, P. Girard, and G. Leveque, "Electrostatic forces acting on the tip in atomic force microscopy: Modelization and comparison with analytic expressions," *J. Appl. Phys.*, **81**, 1023-1030 (1997).

[20]G. Koley, M. G. Spencer, and H. R. Bhangale, "Cantilever effects on the measurement of electrostatic potentials by scanning Kelvin probe microscopy," *Appl. Phys. Lett.*, **79**, 545-547 (2001).

[21]D. S. H. Charrier, M. Kemerink, B. E. Smalbrugge, T. de Vries, and R. A. J. Janssen, "Real versus measured surface potentials in scanning Kelvin probe microscopy," *ACS Nano*, **2**, 622-626 (2008).

[22]S. Guriyanova, D. S. Golovko, and E. Bonaccurso, "Cantilever contribution to the total electrostatic force measured with the atomic force microscope," *Meas. Sci. Technol.*, **21**, 025502 (2010).

[23]A. Efimov and S. R. Cohen, "Simulation and correction of geometric distortions in scanning Kelvin probe microscopy," *J. Vac. Sci. Technol. A*, **18**, 1051-1055 (2000).

[24] $\partial C_i^{cone} / \partial z = a_1 \exp\left(a_2 \exp\left[a_3 x\right]\right) + a_4 \exp\left(a_5 \exp\left[a_6 x\right]\right)$.

[25]U. Rabe, K. Janser, and W. Arnold, "Vibrations of free and surface-coupled atomic force microscope cantilevers: Theory and experiment," *Rev. Sci. Instrum.*, **67**, 3281-3293 (1996).

[26] $\partial C_i^{cant} / \partial z = \frac{1}{1 + b_1 \exp(b_2 x)}(b_3 x + b_4) + \left(1 - \frac{1}{1 + b_1 \exp(b_2 x)}\right) b_5 \exp(b_6 \exp[b_7 x])$.

[27]B. C. Stipe, H. J. Mamin, T. D. Stowe, T. W. Kenny, and D. Rugar, "Noncontact Friction and Force Fluctuations between Closely Spaced Bodies," *Phys. Rev. Lett.*, **87**, 096801 (2001).

[28]A. A. Chumak, P. W. Milonni, and G. P. Berman, "Effects of electrostatic fields and Casimir force on cantilever vibrations," *Phys. Rev. B*, **70**, 085407 (2004).

[29]D. Rugar, H. J. Mamin, P. Guethner, S. E. Lambert, J. E. Stern, I. McFadyen, and T. Yogi, "Magnetic force microscopy: General principles and application to longitudinal recording media," *J. Appl. Phys.*, **68**, 1169-1183 (1990).

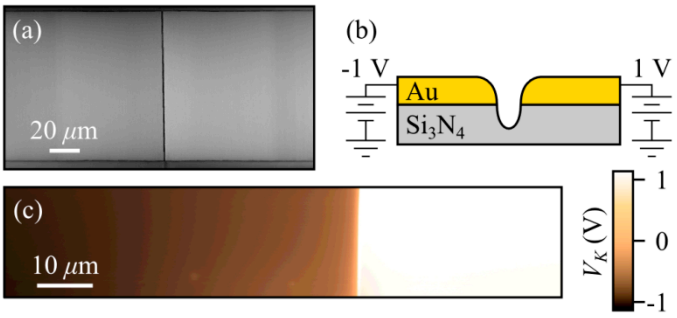

FIG. 1. (Color online) (a) Scanning electron micrograph of a test sample for KPFM. The light strip running left to right is a gold electrode which has been separated into two regions by a narrow cut with a focused ion beam (FIB). The FIB cut is visible as a thin vertical black line in the center of the image. (b) Schematic cross-section of the test sample. The left and right gold regions are electrically isolated and held at -1 V and 1 V, respectively. (c) Image of the Kelvin voltage V_K at the interface between the two gold regions. The plot smoothly and quickly transitions from -1 V on the left to approaching 1 V on the right.

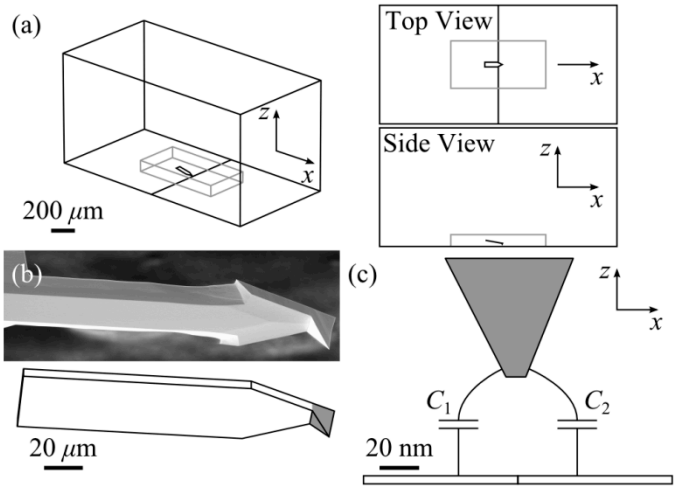

FIG. 2. (a) Schematic of the region used for electrostatic simulation shown in (left) isometric and (right) top and side views. The larger rectangular prism outlined in black and the smaller rectangular prism outlined in gray outline the simulation volumes used for simulations of the cantilever and cone, respectively. The floor of the model is split into two square regions, which act as the sample electrodes. The probe is positioned near the center of the sample. (b) An SEM micrograph of an AFM probe of the same model as the one used in the experiment above a schematic of the probe model used in the simulation, at the same scale. On the schematic, the white section is the cantilever, and the gray section is the cone. (c) Schematic of the electrostatic simulation, side view. The tip of the probe is suspended 50 nm above the two sample electrodes. The capacitance between the probe and the left and right sample electrodes are C_1 and C_2, respectively.

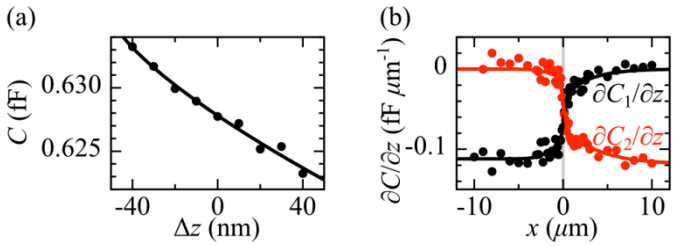

FIG. 3. (Color online) (a) Simulated capacitance C between the cone and an element of the sample *vs*. the change in probe-sample separation Δz. The points are from electrostatic simulations, and the lines are power law fits to the points. (b) The derivative of the cone-sample capacitance $\partial C/\partial z$ *vs*. lateral position x of the cone along the sample. Each point represents the derivative of the power law fit to C vs. Δz for a particular x value. The lines are fit to the sum of two Gompertz functions.

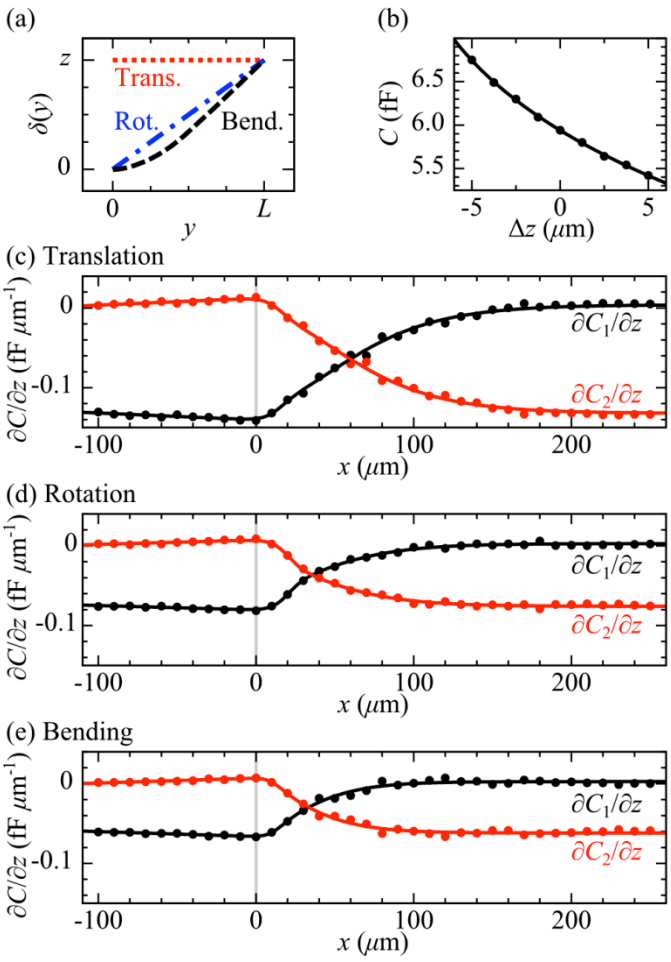

FIG. 4. (Color online) (a) Simulated cantilever deviation δ from rest *vs.* position y along the axis of the cantilever for each of the translation, rotation, and bending profiles. (b) Typical plot of capacitance between the cantilever and a sample element C vs. the change in probe-sample separation Δz, in this case using the translation profile. The points are from electrostatic simulation, and the curve is a power law fit to C *vs.* Δz. (c-e) The derivative of the cantilever-sample capacitance $\partial C/\partial z$ *vs.* lateral position x of the cantilever along the sample. The translation, rotation, and bending models are in use on (c), (d), and (e), respectively. Each point represents the derivative of the power law fit to C *vs.* Δz for a particular x value. The lines are each a linear function times a logistic function added to a Gompertz function times a logistic function, fit to the points.

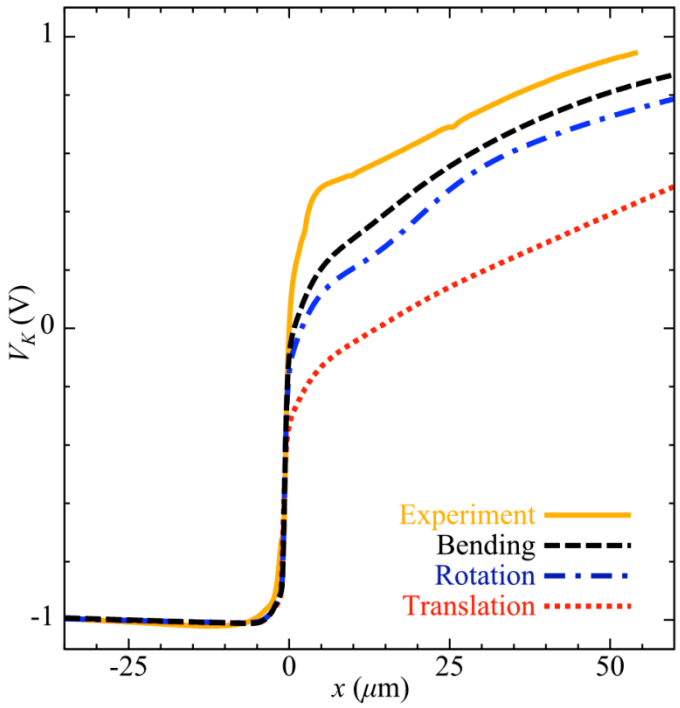

FIG. 5. (Color online) Plot of Kelvin voltage V_K *vs*. lateral position x for the experiment, along with simulation results for the bending, rotation, and translation models. Each curve has -1 V assigned to the left sample electrode and 1 V assigned to the right sample electrode. Allowing the cantilever to bend produces the closest agreement with the experiment.